Catalysis Today 171 (2011) 72–78

Contents lists available at ScienceDirect

Catalysis Today

journal homepage: www.elsevier.com/locate/cattod

Effect of catalyst formulation (Rh, Rh–Pt) on the performance of a natural gas hybrid catalytic burner

S. Cimino[a,*], C. Allouis[a], R. Pagliara[a], G. Russo[b]

[a] Istituto Ricerche sulla Combustione - CNR, Italy
[b] Dipartimento di Ingegneria Chimica Università di Napoli Federico II, Italy

ARTICLE INFO

Article history:
Received 29 October 2010
Received in revised form 3 February 2011
Accepted 16 February 2011
Available online 21 March 2011

Keywords:
Hybrid catalytic combustion
Catalytic partial oxidation
Radiative heat transfer
Diffusive flame
NO_x emissions
Natural gas
Structured catalyst
Rh
Pt

ABSTRACT

An extensive experimental campaign was carried out on a prototype hybrid radiant burner with ultra low emissions based on the novel concept of fuel-rich catalytic + homogeneous flame combustion with inter-stage heat transfer. Special attention was paid to the impact of two alternative active formulations for the catalytic partial oxidation stage (0.5% Rh and 0.25–0.25% Rh–Pt on γ-Al_2O_3) on the general performance of the burner, and particularly on its NO_x emissions. The hybrid burner was operated with methane in the 4–30 kW power range, at varying the feed equivalence ratio ϕ from 2.0 to 3.6. InfraRed thermography was used to simultaneously investigate the catalytic surfaces and the corresponding subsequent diffusion flames. Moreover this work attempts to correlate detailed experimental data on syn-gas compositions at the exit of the CPO reactor with emissions in the exhaust. Experimental evidence of the reduction of both thermal and prompt NO_x formation mechanism is presented.

1. Introduction

An increasing concern regarding environmental pollution during the last years has resulted in stricter emission regulations for NO_x, CO and greenhouse gases form combustion processes. In particular, due to the increasing use of natural gas (NG) to meet the world's energy demand, large research efforts are devoted to the reduction of NO_x emissions and increase of safety and efficiency in NG combustion appliances at both industrial and domestic level [1–3]. Currently, both industrial and utility gas turbine manufacturers prefer lean-premixed combustion technology which has demonstrated the ability to achieve an impressive reduction in NO_x emissions during operation on natural gas [1]. A similar picture is also valid for non-adiabatic (radiant) burners for domestic and industrial applications [2]. As flame temperatures are reduced to achieve these levels of emission performance, flame stability and safety issues may arise [1].

Premixed catalytic combustion technology can guarantee the lowest NO_x emissions compared to other combustion options [2,4], but it has not reached a widespread use mainly due to the lack of a single catalyst capable to fulfil all the requirements in terms of high activity, thermal and mechanically stability, long term durability and low cost [4]. A novel approach has been proposed for gas turbine burners based on a fuel-rich catalytic/lean homogeneous combustion technology [1], which offers benefits in terms of improved safety and stability of operation with respect to lean premixed catalytic and non-catalytic combustion, associated to ultra low pollutants emissions [1,5].

Recently we have extended the concept of fuel-rich catalytic combustion proposing a novel staged hybrid catalytic gas burner, with integrated interstage heat removal by IR radiation from the hot catalytic reactor/radiator [6]. A first prototype burner with a structured Rh/Al_2O_3 catalytic partial oxidation (CPO) stage followed by a purely diffusive flame has proved to guarantee significant enhancements with respect to the state-of-the-art fully premixed or blue-flame diffusive gas burners for domestic condensing boilers [6].

In fact, a number of catalysts have been tested for the CPO of hydrocarbons from methane up to diesel and jet-fuels and Rh-based catalysts have shown the highest activity and selectivity to syn-gas [7–9]. However, the presence of sulphur bearing compounds added as odorants to pipe-line natural gas, was shown to reduce the CPO activity by partial inhibition of steam reforming reaction path [10,11]. The partial substitution of Rh with Pt was reported as effective both at reducing the cost and limiting the detrimen-

* Corresponding author at: P. le V. Tecchio 80, 80125 Napoli, Italy.
Tel.: +39 081 7682233; fax: +39 081 5936936.
E-mail address: stefano.cimino@cnr.it (S. Cimino).

0920-5861/$ – see front matter © 2011 Elsevier B.V. All rights reserved.
doi:10.1016/j.cattod.2011.02.018

tal impact of S on monometallic Rh catalyst [12]. The improved S-tolerance of the bimetallic Rh–Pt catalyst is due to its higher operating temperature all conditions being equal [12]; such feature could be advantageous also for the specific application in hybrid catalytic combustion, whose effectiveness relies on the transfer of reaction heat by radiation from the hot catalytic surface.

Accordingly, we set out to study the impact of two catalytic formulations (namely 0.5% Rh and 0.25–0.25% Rh–Pt on γ-Al_2O_3) on the main features and NO_x emissions performance of the prototype catalytic hybrid burner in its simplest configuration with a purely diffusive secondary flame. The burner was operated at atmospheric pressure on methane (main component of NG and most difficult hydrocarbon to oxidize catalytically) in the 4–30 kWth power (P) range, at varying the feed equivalence ratio ϕ from 2.0 to 3.6. In particular this work used InfraRed thermography to simultaneously investigate the catalytic surface and the characteristics of the corresponding flame, and makes an attempt to correlate detailed experimental data on gas compositions at the exit of the CPO reactor with the emissions in the exhaust from the flame.

2. Experimental

2.1. Catalyst preparation and characterization

Structured catalytic elements were prepared starting from a metallic gauze made of a high temperature FeCrAlloy knitted wire ($d \approx 120$ μm) produced by Riello in the form of flexible cylindrical sockets [13] (external diameter $D = 80$ mm, effective height $H = 80$ mm, thickness 2 mm, apparent density 0.38 g/cm^2). The substrates were accurately cleaned, oxidized in air at 800 °C to start to develop the characteristic superficial protective alumina layer on the alloy, and finally washcoated with 3% La_2O_3-stabilized γ-Al_2O_3 (SCFa140-L3 Sasol, 140m^2/g,) applied by a dip-coating procedure [6]; the target alumina loading of ~7 wt.% was obtained with two deposition cycles followed by calcination in air at 800 °C for 3 h.

Fig. 1a and b presents SEM images of the coated FeCrAlloy gauze at different magnifications, revealing the presence of a well adhering porous layer on the metallic wire with an average thickness in the range 7–14 μm; some washcoat accumulation was also noticed in correspondence of bundles of closely packed wires, whereas limited uncoated areas could be found in correspondence of strong bending.

Monometallic Rh catalysts were prepared via incipient wetness impregnation onto washcoated FeCrAlloy gauzes using an aqueous solution of $Rh(NO_3)_3$ (Aldrich) to achieve the desired loading of 0.5 wt.% (metallic substrate excluded). After impregnation, the catalysts were dried at 120 °C and calcined in air at 550 °C. Bimetallic Rh–Pt catalysts were prepared by sequentially impregnating calcined Rh samples (with Rh loading 0.25 wt.%) with a solution of H_2PtCl_6. The target Rh/Pt weight ratio was 1 and the total nominal metal loading was 0.5 wt.% with respect to the applied alumina layer.

2.2. Burner configuration and combustion tests

The hybrid catalytic burner under typical operation together with a rendering of its longitudinal section is presented in Fig. 2: the fresh gas mixture flowed radially through a distributor, the CPO gauze reactor and then into the flame [6]. The hybrid burner was tested in upward position and secondary air for flame combustion was withdrawn by natural convection from the surroundings.

Pure methane and compressed air flows were regulated by two independent mass flow controllers and mixed at atmospheric pressure. Combustion tests were always performed with a fuel rich mixture fed to the burner at an equivalence ratio ϕ variable in the range 2.0–3.6 (i.e. above upper flammability limit). The nominal thermal power was varied between 3.8 and 29 kW based on the lower heating value of methane. The resulting gas hourly space velocity (GHSV) at room temperature was comprised between 0.1×10^6 and 1.0×10^6 h^{-1}, referred to the empty volume of the catalytic mesh, corresponding to a contact time between 0.9 and 10 ms at the reaction temperature.

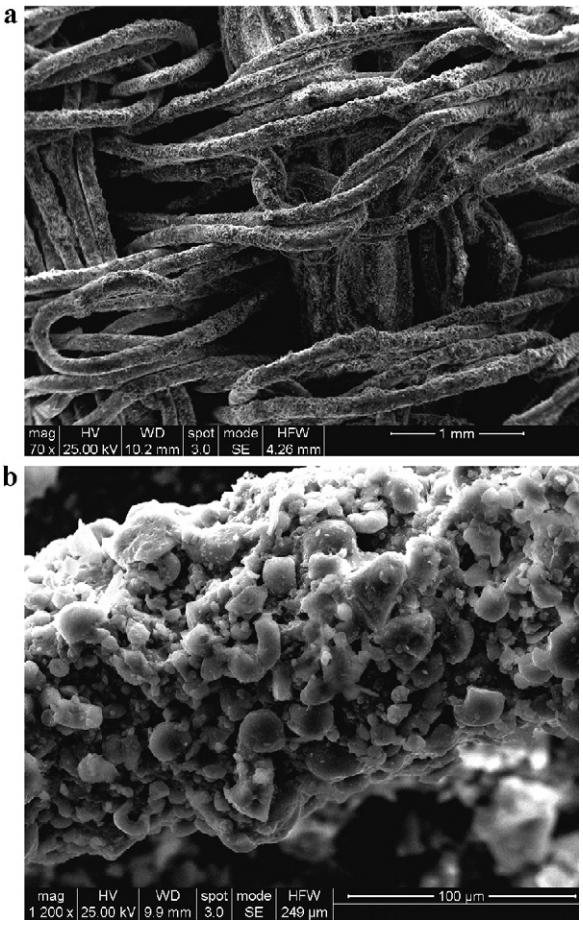

Fig. 1. SEM images at increasing magnifications of the FeCrAlloy knitted gauze substrate (a) after deposition of the γ-Al_2O_3 layer, and close-up view of the washcoated metallic wire (b).

InfraRed thermography was selected as a fast, not-intrusive, flexible measurement tool to investigate the hybrid burner and to obtain simultaneously the temperature profile on the catalytic surface and an estimation of the flame temperature and structure. Two FLIR thermocameras were employed: a Phoenix with digital acquisition system, and a SC500, respectively, with spectral sensitivities in the range 1.5–5 μm and 7.5–12 μm. Independent thermocouple measurements were preliminary performed to set appropriate emissivity factors, which were checked against literature ranges [14–19]. Further calibration tests were performed for the Phoenix camera using a black body up to 1700 K. In particular, two optical spectral filters centred at 3.4 or 3.9 μm were applied on the Phoenix camera in order to eliminate flame (gas) emissivity when measuring the surface temperature of the catalyst; a further filter at 4.25 μm was used to estimate CO_2 (flame) temperature [19]. Moreover, the flame images filtered at 3.9 μm allowed us to identify the possible presence of soot formation. All the IR pictures presented hereafter represent a 5 s-average of the images collected at 340 frames/s.

The temperature of the syn-gas emerging from the catalytic stage was also measured with a shielded (Inconel 600, $d = 0.5$ mm)

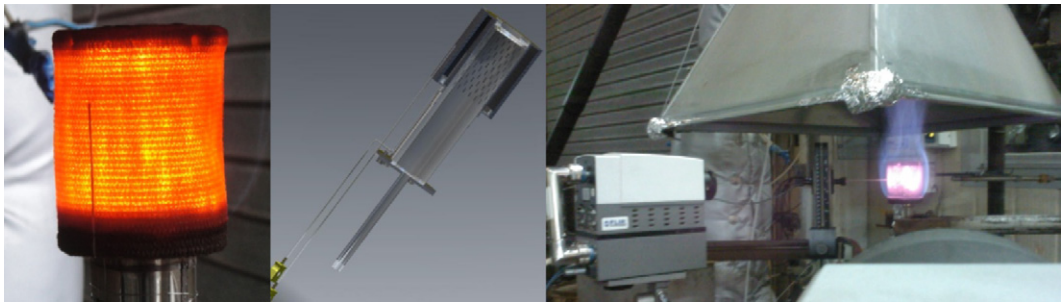

Fig. 2. Picture of the catalytic combustion head ($D \times L = 80\,\text{mm} \times 80\,\text{mm}$) under typical operation (left), rendering of its longitudinal section (centre), and a view of the experimental set-up for IR thermography (right).

K-type thermocouple placed 1 mm downstream from the catalyst surface and parallel to it.

Gas analysis was performed in real time with ABB Advance Optima instruments equipped with ND-IR/-UV, TC and paramagnetic detectors (respectively, for CH_4, CO, CO_2; NO, NO_2; H_2; O_2). The effluent gas from the catalytic partial oxidation stage was sampled with a cooled stainless steel probe in close contact with the surface of the catalytic gauze.

Methane conversion and selectivities to CO and H_2 were calculated according to the definitions:

$$x_{CH_4} = 100\left(1 - \frac{CH_4^{out}}{CH_4^{out} + CO_2^{out} + CO^{out}}\right)$$

$$S_{CO} = 100\left(\frac{CO^{out}}{CO_2^{out} + CO^{out}}\right)$$

$$S_{H_2} = \frac{100}{2}\left(\frac{H_2^{out}}{CO_2^{out} + CO^{out}}\right)$$

based on exit dry-gas mol fractions of CH_4, CO, CO_2, and H_2 from the CPO reactor.

Exhaust gases from the burner were collected by a hood and the emissions of CO, NO_x and CH_4 were corrected to 0% O_2 conditions.

Adiabatic flame temperatures were calculated using CHEMKIN 4.1.1 software [20] assuming a stoichiometric flame, based on the measured compositions and temperatures of the effluent gas streams from the CPO stage with both catalytic formulations.

3. Results and discussion

IR analysis of the hybrid burner (Fig. 3) showed the presence of an axial-symmetric laminar diffusive flame structure surrounding the hot radiating catalytic reactor, which had a very uniform temperature distribution on the whole outer surface. The flame itself, which appeared blue and had a low-luminosity, was found to be non-sooting, as confirmed by careful inspection of IR images collected at $F = 3.9\,\mu m$ in the gas phase surrounding the burner (Fig. 3b).

Hot gas leaving the combustion head through the catalytic gauze was slightly colder than the catalyst itself. This was also confirmed by the thermocouple measurements [6] and implies that, inside the structured catalytic layer, heat generation occurs through surface oxidation reactions and the flowing gases are only heated by convection. Moving away from the catalytic surface along the radial coordinate we observed an initially flat temperature profile in the gas phase due to the absence of oxidation reactions close to the head: all of the oxygen from primary air was consumed by catalytic oxidation reactions (see next section), and more O_2 from the surrounding air had to diffuse to complete combustion. Thereafter T_{gas} raised to a maximum in correspondence of a symmetric laminar diffusion flame front developed around the burner and above it, which was well captured by CO_2 profiles (F 4.25 μm). However, it should be underlined that temperature profiles in the gas phase were obtained by measuring the characteristic emission of CO_2 at 4.25 μm, therefore they are only qualitative due to: varying CO_2 concentration, spatial integration of the emission, flame thickness, presence of an emitting/adsorbing/reflecting surface behind the flame [19] (which was particularly evident for low values of ϕ as in Fig. 3c, i.e. when the catalyst ran hotter).

The laminar flame envelope expanded at higher input power (and lower ϕ), due to the corresponding higher flow rate and exit velocity of the gas leaving the catalytic head in the radial direction, which pushed the diffusive flame front away from the catalyst. Since the catalyst was hotter at lower values of ϕ, it also preheated the reformed exit gas to a large extent. It is also clear that the flame front extended well above the catalytic head, due to the relatively slow diffusion of oxygen from the surroundings and to poor mixing effectiveness with secondary air achieved by natural convection.

The hybrid catalytic burner performs a staged combustion, and is characterized by interstage heat transfer by IR radiation from the hot catalytic head to a heat sink. By this way the peak temperature reached at the diffusion flame front can be strongly reduced. This is shown in Fig. 4a and b which reports the temperatures measured on the outer surface of the two catalytic gauzes as a function of ϕ and for 3 nominal power levels, together with the corresponding adiabatic flame temperatures calculated from the measured composition of the syn-gas leaving the catalytic stage. For both catalysts the outer surface temperatures were comprised in the range 650–1050 °C, strongly increasing with decreasing ϕ, due to a larger availability of the limiting reactant (oxygen) for the heterogeneous oxidation reactions. Higher temperatures were also measured at constant ϕ for a higher nominal power (i.e. flow rate) to the burner: this is a well recognized feature of non-adiabatic CPO reactors, because heat loss does not scale with flow rate as long as the contact times are adequately long to maintain full O_2 conversion [9].

Moreover a temperature profile (not shown) developed in the very short (2 mm) catalytic reactors, with peak temperatures (controlled by ϕ) located in the entrance (oxidation) zone of the gauze, which progressively moved downstream towards the outer radiating face at increasing gas flow rates [6].

From Fig. 4 it appears that the bimetallic catalyst always ran 50–100 °C hotter than its monometallic Rh counterpart at any fixed P level, which also precluded to explore very low ϕ values in order to prevent catalyst overheating and deactivation. It was already reported that substitution of half of the Rh loading with same weight amount of Pt entails a significant increase in the operating temperatures of methane CPO monoliths, since reactions leading to total oxidation products become more important on Pt [12]. In fact the higher syn-gas yield on Rh catalyst is strictly asso-

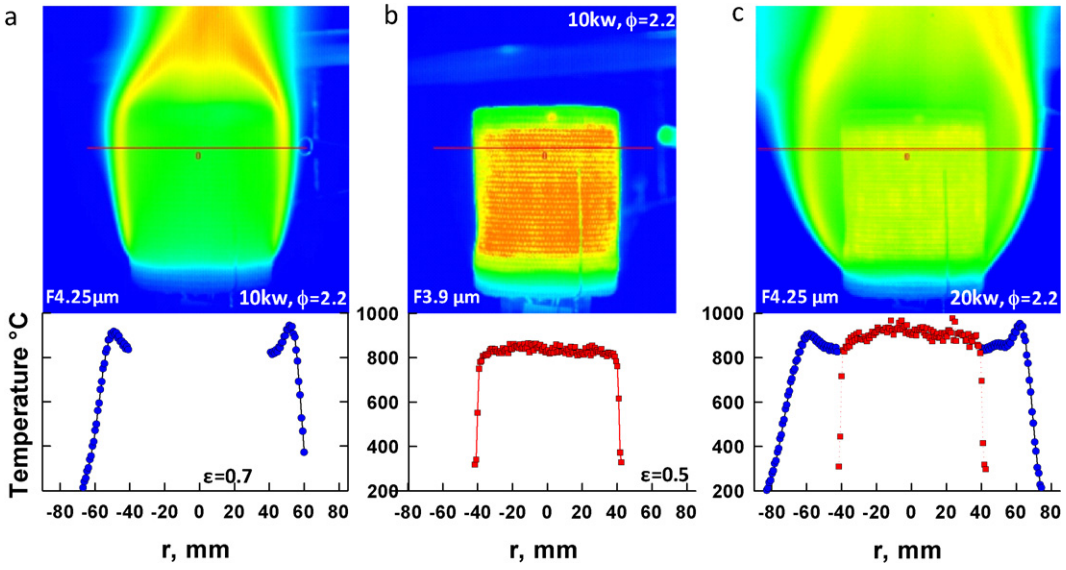

Fig. 3. InfraRed images of the flame structure (CO_2) and of the catalytic surface collected at 4.25 μm and 3.9 μm, respectively, together with the corresponding temperature profiles at fixed height along the line shown in figure. Rh catalyst operated at $\phi = 2.2$: (a) $P = 9.6$ kW, $F = 4.25$ μm; (b) $P = 9.6$ kW, $F = 3.9$ μm; (c) $P = 19.2$ kW, $F = 4.25$ μm.

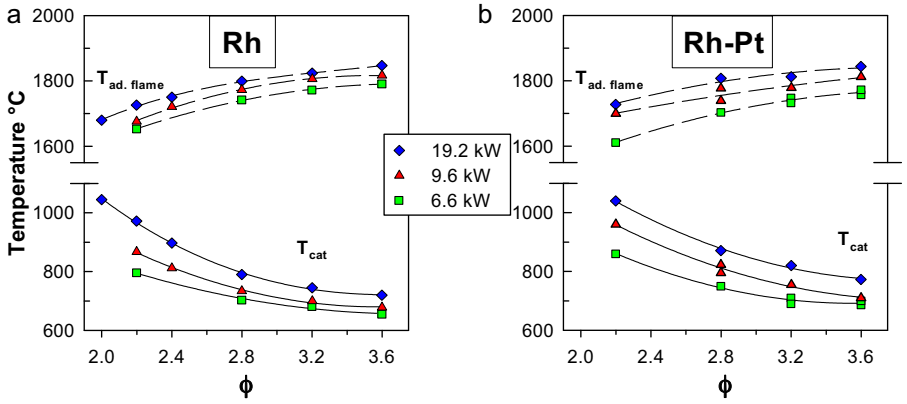

Fig. 4. Temperature of the outer catalytic surface and corresponding adiabatic flame temperature of the emerging syn-gas for Rh (a) and Rh–Pt (b) catalysts as a function of ϕ at different power levels.

ciated to its higher activity for the endothermic methane steam reforming reaction whose contribution is significant even at very short contact times [8,10], and strongly non-adiabatic conditions [6,11].

As shown in the upper part of Fig. 4a,b, the adiabatic flame temperature of the syn-gas follows an opposite trend with respect to the catalyst temperature, progressively decreasing for lower ϕ values, as a consequence of the larger quantity of heat transferred by radiation from the hotter catalytic surfaces. However, at fixed ϕ, the adiabatic flame temperature increases with the nominal input power due to a reduction in the percentage of heat loss from the CPO reactor. In fact, the fraction of thermal power emitted by the hot radiating catalyst decreased progressively for higher values of the input power, although its absolute value increased due to higher surface temperatures [6].

3.1. Catalytic partial oxidation stage

Fig. 5a–e compares the catalytic activities of supported Rh and Rh–Pt catalysts during the CPO of methane as a function of the feed equivalence ratio ϕ for several Power levels. Gas analysis at the exit of the CPO reactor confirmed that O_2 conversion was always complete on both catalysts for all conditions explored [6,8–12], whereas no sign of NO_x formation could be found.

Methane conversion and selectivities to CO and H_2 followed the general trends predicted by thermodynamic equilibrium calculations (solid lines in Fig. 5) under adiabatic conditions, departing from them in a measure depending on both the active phase composition and the specific input power level (P).

Monometallic Rh catalyst showed the best performance in terms of methane conversion, which increased steadily with decreasing ϕ, respectively, exceeding 90% for $\phi \leq 3.0$ and 99% for $\phi \leq 2.2$, whereas it was almost unaffected by the value of P in the range explored. Partial substitution of Rh with Pt entailed a reduction in fuel conversion by roughly 5 percentage points for values of ϕ down to 2.4, leaving about 2–3% of unconverted methane also at $\phi = 2.2$. Moreover Rh catalyst showed a higher selectivity to both CO and H_2, which is particularly evident when comparing the relevant plots at lower values of power. However, similar selectivities to syn-gas were measured on the two catalysts at the highest values of P, as a consequence of the higher associated operating temperatures (Fig. 4) leading to a closer approach to thermodynamic equilibrium values.

To sum up, the fuel for the second stage of homogeneous combustion was constituted by a hot, low-heating value syn-gas stream, whose typical composition is reported in Table 1 for each catalyst and for two values of ϕ ($P = 9.6$ kW). The relatively high content of H_2 in the syn-gas peaked at $\phi = 2.8$ with both catalysts, and the H_2/CO ratio increased with ϕ in the range 1.55–1.75. Lower ϕ values

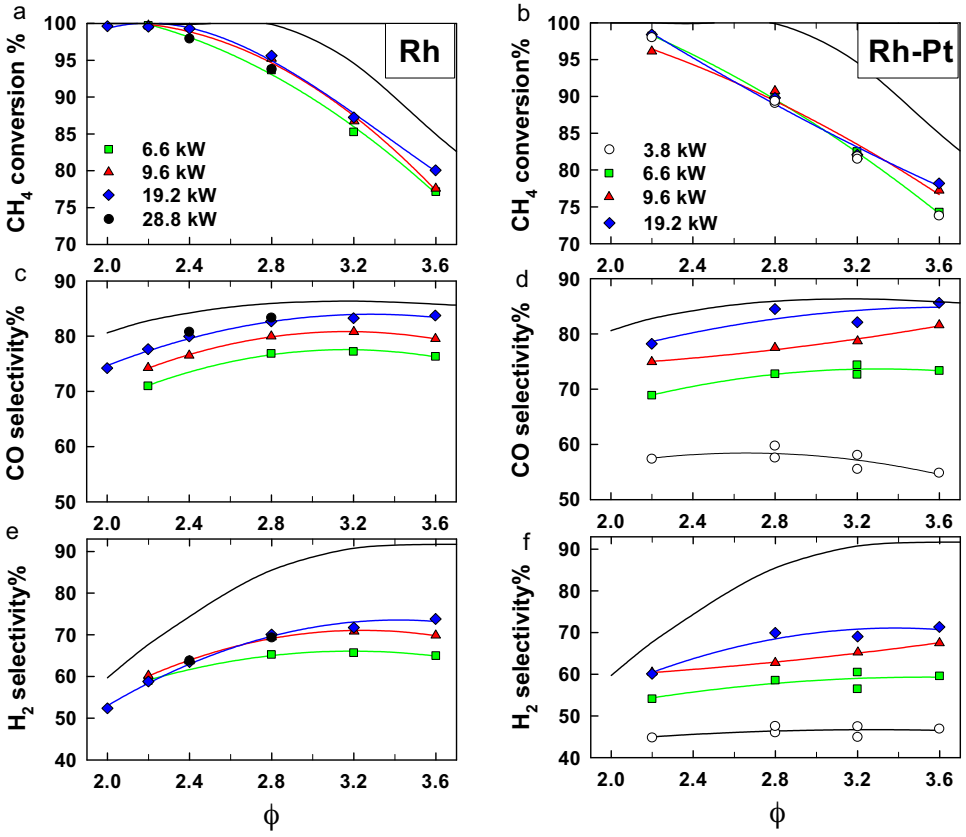

Fig. 5. Methane conversion (a, b), CO (c, d) and H_2 (e, f) selectivities as a function of ϕ at several nominal power levels. Rh (left panels) and Rh–Pt (right panel). Solid lines represent thermodynamic (p, H = constant) equilibrium values.

Table 1
Comparison of the compositions (mol.%) of syn-gases produced by CPO of methane on 0.5% Rh and 0.25–0.25% Rh–Pt catalysts.

P = 9.6 kW	ϕ = 2.8		ϕ = 2.2	
	Rh	Rh–Pt	Rh	Rh–Pt
CH_4 (%)	0.85	0.61	0.04	1.65
H_2 (%)	23.58	18.26	18.66	22.43
CO (%)	13.58	11.32	11.51	12.96
H_2O (%)	10.38	11.95	12.34	10.81
CO_2 (%)	3.40	3.79	3.99	3.50
N_2 (%)	48.21	54.08	53.47	48.97
T_{out} (°C)	581	695	655	618

allowed a reduction of the differences between syn-gas compositions from the two catalysts and also increased the dilution level, with N_2 from primary combustion air accounting for more than 50% of the mixture, steam for 10–12% and CO_2 for 3–4%.

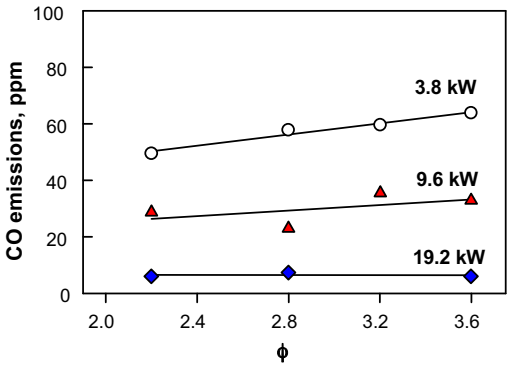

Fig. 6. CO emissions corrected @0% O_2 from the hybrid burner with bimetallic Rh–Pt catalyst as a function of ϕ at different power levels.

3.2. CO and CH_4 emissions

Fig. 6 reports CO emissions measured for the hybrid burner with bimetallic catalyst, which are also representative of the monometallic Rh system. CO concentration was always ≤60 ppm (corrected @0% O_2), and was weakly affected by ϕ only at low-mid input power levels, where it slightly decreased if more primary air was fed to the catalyst. At the same time, unburned CO decreased strongly at higher power levels (6–7 ppm at 19.2 kW), suggesting that most of the emissions were due to local quenching effects possible at low flow rates, when the diffusive laminar flame front was placed very close to the catalytic combustion head. Moreover CH_4 emissions in the exhaust were always below the detection limit (10 ppm) with both catalysts and for the whole range of conditions explored, confirming our previously reported results [6]. Syn-gases with dominant carbon monoxide and hydrogen fractions present a much wider ignition range than those of conventional hydrocarbon fuels of natural gas [21]. In the hybrid burner the operational range for homogeneous combustion is further expanded by the high preheating of the fuel produced in the catalytic stage and by its high H_2 content, which facilitates the oxidation of other organic fuel fractions. Both circumstances effectively lower the probability of unburned gas eddies of improper mixing, resulting in low emissions of unburned CO and methane, even in systems with poor mixing judged by the standard of conventional design [21].

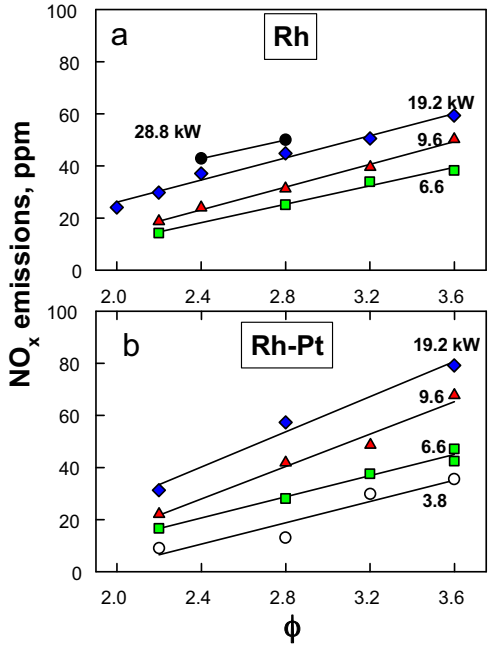

Fig. 7. Total NO_x emissions corrected @0% O_2 form hybrid burner with Rh (a) and Rh–Pt (b) catalyst as a function of ϕ at different power levels.

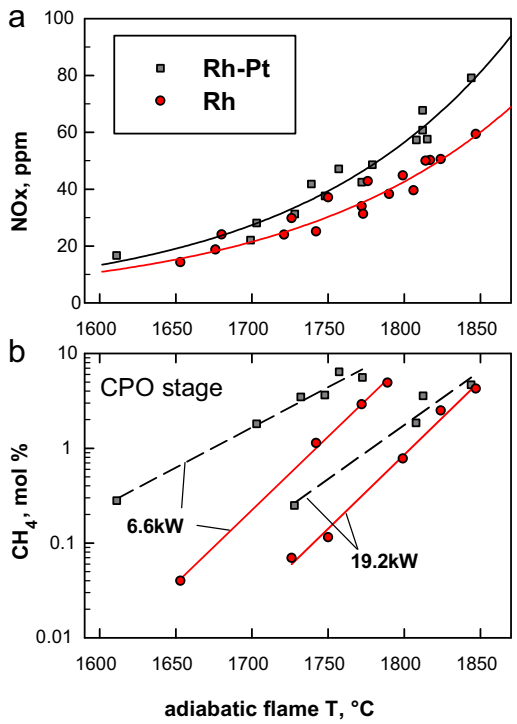

Fig. 8. (a) Total NO_x emissions corrected @0% O_2 produced by the hybrid burner with Rh and Rh–Pt catalysts as a function of the adiabatic flame temperature of the syn-gas produced. (b) Comparison of the residual methane mol fractions in the syn-gas from the two catalysts for two nominal power levels.

3.3. NO_x emissions

Since no evidence of NO_x formation could be detected at the exit of the catalytic partial oxidation stage, NO_x emissions from the hybrid burner are only due to the homogeneous flame combustion stage: in the simple current configuration, syn-gases emerging from the catalytic gauze were burned under purely diffusive and laminar conditions.

Fig. 7a–b reports the emissions of NO_x (@0% O_2) as a function of ϕ at different power levels for the two catalytic formulations tested. In both cases NO_x concentrations in the exhaust decreased almost linearly with decreasing ϕ, following the same trend of the adiabatic flame temperature of the syn-gas, which was progressively lowered by the increase of interstage heat removal through radiation. Moreover, along with the general increase in the flame temperature levels with the nominal power, also NO_x emissions increased, ranging from 10 to 60 ppm and from 10 to 80 ppm for Rh and Rh–Pt catalysts, respectively. In fact, at any fixed power level, monometallic Rh catalyst guaranteed a significant reduction in NO_x emissions over its bimetallic counterpart.

As a general figure, emissions of NO measured at the exhaust of two commercial burners, a fully premixed lean surface stabilized device and a blue-diffusive turbulent flame one, ranged, respectively, between 20–60 ppm and 80–120 ppm, when operated with their optimal excess of air between 20 and 30% [6]. It came out that both prototypes of the hybrid catalytic burner were able to outperform state-of-the-art premixed burner in terms of NO_x emissions for ϕ values below 3 (Rh) and 2.8 (Rh–Pt), while a maximum of 40–50% reduction in NO_x was achieved with the monometallic Rh-based catalyst operated at the lowest values of ϕ. This result becomes more impressive considering the purely diffusive and laminar nature of the secondary flame under the current burner configuration.

Previous studies on syn-gas combustion in non-premixed flames reported that the contributions of thermal and prompt mechanisms to total NO_x are comparable while that of N_2O-intermediate and NNH mechanisms were found to be relatively small and negligible [22 and ref. therein]. In line with those findings, we showed that the strong NO_x reduction achieved by the hybrid burner with integrated heat removal from the catalytic head is largely due to the reduction of the peak flame temperatures responsible for thermal NO_x formation. However, NO_x formation through the prompt mechanism is less affected by temperature due to the relatively low activation energy of the initiation reaction step involving CH radical ($CH + N_2 \leftrightarrow HCN + N$) [21,22]. In order to separate the thermal and chemical effects, the NO_x mole fractions in the exhaust from the two catalytic burners are presented in Fig. 8a as a function of the stoichiometric adiabatic flame temperature of the syn-gas from the CPO stage calculated from measured compositions and temperatures (Table 1). When plotted against the adiabatic flame temperature, all of the scattered emission data reported in Fig. 7 collapse in single curves for each catalyst formulation, showing a relatively weak exponential growth with Tad, suggesting a minor role played under such conditions by thermal NO_x with respect to prompt formation mechanism.

For the same adiabatic flame temperature of the syn-gas, monometallic Rh catalyst constantly guaranteed a further 20–25% NO_x reduction with respect to its bimetallic counterpart. In order to explain this behaviour Fig. 8b compares the residual CH_4 mole fractions in the syn-gas produced on each of the two catalysts as a function of the adiabatic flame temperature at two power levels. Since a lower fuel conversion in the CPO stage entails an increase in the adiabatic temperature of the subsequent flame, it follows that methane concentration in syn-gas increases progressively along with T_{ad}. From Fig. 8a and b it appears that the superior performance of Rh catalyst in terms of lower unconverted methane reflects in a lower formation of prompt NO_x in the flame. In fact it was demonstrated [22] that the presence of relatively small amounts of methane in $CO–H_2$ mixtures increases the formation of acetylene considerably, which causes a significant increase in CH concentration and thereby in prompt NO_x. A higher residual methane concentration in the syn-gas mixture might also adversely affect soot emissions as a consequence of a predicted increase in

acetylene concentration (soot precursor) at high temperature in the flame front [22]. However, non-sooting flames were observed to surround each of the two catalysts. In fact, the large concentration of diluents (N_2, H_2O, CO_2, see Table 1) in the syn-gas fuel prepared by the CPO stage also entailed a beneficial effect for further prompt NO_x, as well as soot, suppression. H_2O, and to a lower extent CO_2, were reported to have a chemical effect that, for the same peak flame temperature, reduces the concentrations of CH and C_2H_2 [23,24].

4. Conclusions

Hybrid catalytic combustion technology is based on a short contact time catalytic partial oxidation reactor operating at high temperature (600–1050 °C): the structured catalyst directly transfers a significant portion of the heat of reaction by radiation while preparing a syn-gas fuel for the subsequent flame combustion. To reach this goal, monometallic Rh and bimetallic Rh–Pt on γ-alumina catalysts were anchored onto structured substrates made of a FeCrAlloy knitted wire gauze and tested in a radial flow radiant burner operated on methane with a purely diffusive secondary flame. Both catalysts were able to steadily convert methane with high fuel conversion and selectivities to H_2 and CO under strongly non-adiabatic conditions. The higher (reforming) activity of Rh determined a higher conversion to syn-gas on the monometallic catalyst, whereas the partial substitution with Pt slightly favoured total oxidation products, therefore sustaining higher surface temperatures (and radiative heat transfer) for the same value of the equivalence ratio ϕ. Indeed, it was possible to finely control the maximum temperature of the catalysts by simply acting on ϕ. Moreover, the adiabatic flame temperature of the produced syn-gas was significantly reduced and followed an opposite trend with respect to the temperature of the catalyst, progressively decreasing for lower ϕ values. The hot, diluted, and highly reactive syn-gas from the CPO stage was finally burned in a laminar diffusive flame, which was found to be non-sooting and to produce very low emissions of CO and CH_4, even in a systems with poor mixing. Regarding NO_x emissions, the contribution from thermal formation mechanism was strongly limited due to the significant reduction of the peak flame temperature. Prompt NO_x were also limited due to the high dilution of the syn-gas, which contained low amounts of unreacted hydrocarbons and high concentrations of H_2O and CO_2. It came out that the prototype hybrid catalytic burner was able to outperform state-of-the-art lean premixed burners in terms of NO_x emissions with as much as 50% reduction achieved with the monometallic Rh catalyst operated at the lowest values of ϕ. For the same adiabatic flame temperature of the syn-gas, the monometallic Rh catalyst always guaranteed a 20–25% NO_x reduction with respect to its bimetallic counterpart, because of a lower contribution from prompt NO_x formation mechanism due to the lower concentration of residual methane in the syn-gas.

Acknowledgment

This work was supported by the "MSE-CNR Accordo di Programma per l'Attività di Ricerca di Sistema, project: Gas Naturale/Biocombustibili".

References

[1] B. Bairda, S. Etemad, H. Karim, S. Alavandi, W.C. Pfefferle, Catal. Today 155 (2010) 13–17.
[2] S. Specchia, A. Civera, G. Saracco, V. Specchia, Catal. Today 117 (2006) 427–432.
[3] S. Specchia, G. Toniato, Catal. Today 147 (2009) S99–S106.
[4] P. Forzatti, Catal. Today 83 (2003) 3–18.
[5] L. Smith, H. Karim, M. Castaldi, K. Lyle, S. Etemad, W. Pfefferle, V. Khanna, K.J. Smith, Eng. Gas Turbines Power 127 (2005) 27.
[6] S. Cimino, G. Russo, C. Accordini, G. Toniato, Combust. Sci. Technol. 182 (2010) 380–391.
[7] B. Enger, R. Lødeng, A. Holmen, Appl. Catal. A: Gen. 346 (2008) 1–27.
[8] R. Horn, K.A. Williams, N.J. Degenstein, A. Bitsch-Larsen, D. Dalle Nogare, S.A. Tupy, L.D. Schmidt, J. Catal. 249 (2007) 380.
[9] S.-A. Seyed-Reihani, G.S. Jackson, Catal. Today 155 (2010) 75–83.
[10] A. Bitsch-Larsen, N.J. Degenstein, L.D. Schmidt, Appl. Catal. B: Environ. 78 (2008) 364–370.
[11] S. Cimino, R. Torbati, L. Lisi, G. Russo, Appl. Catal. A: Gen. 360 (2009) 43.
[12] S. Cimino, L. Lisi, G. Russo, R. Torbati, Catal. Today 154 (2010) 283–292.
[13] A. Lovato, G. Toniato, European Patent EP1544542, 2005.
[14] L.S. Bernstein, D.C. Robertson, J.A. Conant, J. Quant. Spectrosc. Radiat. 23 (1980) 169–185.
[15] J. Spelmana, T.E. Parkera, C.D. Carter, J. Quant. Spectrosc. Radiat. 76 (2003) 309–330.
[16] G. Parent, Z. Acem, S. Lechene, P. Boulet, Int. J. Therm. Sci. 49 (2010) 555–562.
[17] HITRAN., database, 1992 ed., V. 2.41 based on L.S. Rothman, et al., J. Quant. Spectrosc. Radiat. 48 (1992) 469.
[18] M. Golombok, L.C. Shirvill, Appl. Optics 27 (1988) 3921–3925.
[19] L. Brahmi, T. Vietoris, J.L. Torero, P. Joulain, Meas. Sci. Technol. 10 (1999) 859–865.
[20] R.J. Kee, F.M. Rupley, J.A. Miller, M.E. Coltrin, J.F. Grcar, E. Meeks, H.K. Moffat, A.E. Lutz, G. Dixon-Lewis, M.D. Smooke, J. Warnatz, G.H. Evans, R.S. Larson, R.E. Mitchell, L.R. Petzold, W.C. Reynolds, M. Caracotsios, W.E. Stewart, P. Glarborg, C. Wang, O. Adigun, Chemkin Collection, Release 4.0, Reaction Design, Inc., San Diego, CA, 2004.
[21] K.J. Whitty, H.R. Zhang, E.G. Eddings, Combust. Sci. Technol. 180 (2008) 1117–1136.
[22] D.E. Giles, S. Som, S.K. Aggarwal, Fuel 85 (2006) 1729–1742.
[23] S.C. Li, F.A. Williams, Combust. Flame 118 (1999) 399–414.
[24] S. Jahangirian, A. Engeda, I.S. Wichman, Energy Fuels 23 (2009) 5312–5321.